Midinfrared Tunable Laser with Noncritical Frequency Matching in Box Resonator Geometry

Kunpeng Jia,[1,*] Xiaohan Wang,[1,*] Jian Guo,[1] Yihao Li,[1] Xin Ni,[1] Pengfei Fan,[1] Qiqi Shen,[3] Tao Wang,[4] Xinjie Lv,[1] Gang Zhao,[1] Shu-Wei Huang,[2] Xueming Yang,[3,4] Zhenda Xie,[1,†] and Shi-ning Zhu[1,‡]

[1]*National Laboratory of Solid State Microstructures, School of Electronic Science and Engineering, College of Engineering and Applied Sciences, School of Physics, and Collaborative Innovation Center of Advanced Microstructures, Nanjing University, Nanjing 210093, China*

[2]*Department of Electrical, Computer and Energy Engineering, University of Colorado Boulder, Boulder, Colorado 80309, USA*

[3]*State Key Laboratory of Molecular Reaction Dynamics, Dalian Institute of Chemical Physics, Chinese Academy of Sciences, Dalian, Liaoning 116023, China*

[4]*Department of Chemistry, College of Science, Southern University of Science and Technology, Shenzhen, Guangdong 518055, China*

(Received 26 March 2021; accepted 15 October 2021; published 18 November 2021)

Monolithic optical parametric oscillators extend laser frequencies in compact architectures, but normally guide and circulate all pump, signal, and idler beams. Critical frequency matching is raised among these resonances, limiting operation stability and continuous tuning. Here, we develop a box resonator geometry that guides all beams but only resonates for signal. Such noncritical frequency matching enables 227 GHz continuous tuning, with sub-10 kHz linewidth and 0.43 W power at 3310 nm. Our results confirm that monolithic resonator can be effectively used as a tunable laser including midinfrared wavelength, as further harnessed with methane fine spectral measurement at MHz accuracy.

DOI: 10.1103/PhysRevLett.127.213902

Tunable lasers are essential for high resolution spectroscopy applications at all wavelength ranges [1–4], with the narrow linewidth for high spectral resolution and continuous tuning for gapless spectral coverage. High-performance tunable lasers are well developed at specific wavelengths in the visible–near-infrared (NIR) range, with narrow linewidth down to kilohertz level, broadband mode-hop-free tuning and high output power [5–9]. However, there are other wavelengths that are challenging to match such high laser performance in the linewidth, tuning capabilities and power. These wavelengths may also have special interest, and one good example is the midinfrared (MIR) wavelength from $3 \sim 5$ μm [10,11], which is known as the rotational and vibrational absorption fingerprints of molecules and fulfill the gas spectroscopy requirement [12]. An alternative approach is the indirect laser light generation using the optical parametric oscillation, so that the coherent radiation can be frequency transferred to the target wavelengths using the existing tunable lasers [13–19].

Recent advances of monolithic optical parametric oscillators (OPOs) [20–28] with miniature footprints and high spectral coherence in a compact architecture, pushes forward the development for future field-deployable photonic devices. These monolithic OPOs are not only integrated version of the conventional bulk-element OPOs, but also provides transverse confinement of light via total internal reflection and further lower the threshold. However, the critical frequency matching, which means that the pump laser must match with cavity resonance for efficient coupling, is normally required for their stable operation. This can be more challenging for these monolithic OPOs with their quality factor (Q) scales up. Moreover, such critical frequency matching also well defines output frequencies of the monolithic OPOs, and thus limits their continuous frequency tuning capability as tunable laser. In the case of MIR generation, people still have to use bulk-element OPOs to fulfill the continuous tuning requirement [29–34], which is too bulky, environment sensitive, and expensive for out-of-lab applications.

Here, we develop a new resonator geometry called box resonator for the first demonstration of monolithic mini-OPO with noncritical frequency matching. Such box resonator allows wavelength-selective cavity enhancement, which is key to relaxing the critical frequency matching in a monolithic resonator device, for stable free-running operation and continuous tuning like a tunable laser. It is fabricated by mechanical polishing and dielectric coating, enabling near-material-limited high Q of 2.3×10^7 around 1555 nm. Quasiphase matching (QPM) is engineered by the lithium niobate optical superlattice design, for low-threshold MIR generation around 3.1 μm wavelength with 1 μm pump. By changing the wavelength of the pump laser and temperature of box resonator, a course tuning range over 600 nm is achieved for the single-frequency MIR output, and more importantly, a fine-tuning range of 227 GHz can be performed without mode hops

for continuous MIR coverage. Its uniform and large mode profile further releases the requirement of coupling and allows higher circulating power, for 430 mW high-power MIR output. We further test the MIR source for its spectroscopy capability via the fine absorption features measurement of low-pressure methane, and the result shows megahertz-level spectroscopy accuracy over the whole scan range of 110 GHz. This box resonator can be used as a tunable laser source in the MIR range, with mod-hop-free fine-tuning performance to match that of the visible-NIR tunable laser, for a variety of practical applications.

In quasiphase matched OPO process, the maximum wavelength tuning range is determined by the phase-matching bandwidth, which can be calculated as

$$\Delta v = \frac{0.443}{|\frac{n_{g,p}}{c} - \frac{n_{g,i}}{c}|L}, \tag{1}$$

where $n_{g,p}$ and $n_{g,i}$ are the group index of pump (p) and idler (i) waves, respectively, c and L are the speed of light and the length of box resonator, respectively. However, in the case of doubly and triply resonant configurations, frequency matching between cavity resonances and optical waves adds extra limitation for the continuous tuning, which is not necessarily satisfied and critically sensitive to the cavity dispersion and cavity length in a monolithic OPO. The upper panel of Fig. 1(a) illustrates a conventional triply resonant monolithic resonator such as whispering gallery resonator (WGMR) or microring resonator. Such well-defined frequency matching greatly reduces the continuous tuning range to the resonance linewidth ($\Delta\nu_c$), which is related to the oscillation frequencies (ν) and corresponding cavity Q as $\Delta\nu_c = \nu/Q$. In a triply resonant monolithic OPO with same Q, this value can be calculated to be 3.9 MHz. In addition, such configuration also requires high pump frequency stability in relative to specific resonance. As well known, however, the wavelength-selective resonance can be configured by optical coating for realizing a singly resonant configuration, and here it is applied to a new box resonator geometry as shown in the lower panel of Fig. 1(a). Here, only signal wave around 1550 nm is resonated, so that frequency matching condition is greatly released at pump and idler, and broadband continuous tuning range up to 800 GHz can be expected, which is equal to the phase-matching bandwidth in our box resonator. Based on this principle, the continuous MIR tuning with signal locked at a single resonance can be achieved in such box resonator geometry following the pump tuning.

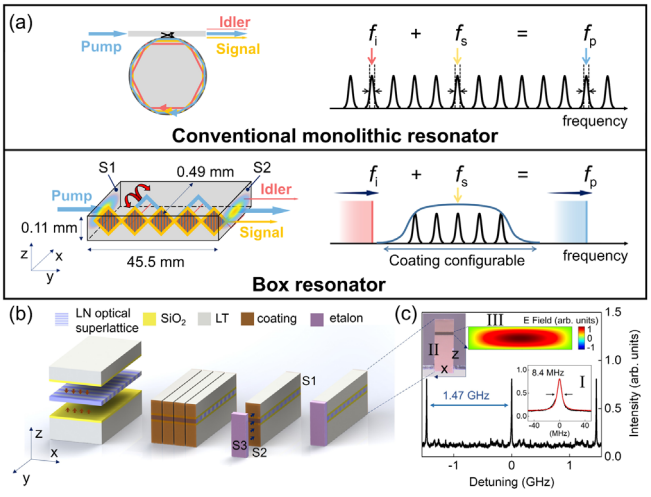

FIG. 1. Box resonator geometry. (a) Schematic of a box resonator in comparison to a conventional monolithic resonator. (b) The fabrication process of a noncritical-frequency-matching box resonator. (c) Box resonator transmission at around 1.5 μm. Inset I shows the fitted resonance linewidth of 8.4 MHz. Inset II shows a microscope photo of surface $S1$. Inset III shows mode profile of TM00 mode.

In this box resonator geometry, high Q at signal wavelength is the key to achieving low threshold, high cavity enhancement, and high efficiency pump to MIR conversion. Previously, material-limited high Q can only be accessed in a mini-OPO via mechanical polishing, and the best example is the WGMR. Here, we revisit this concept by the new box resonator geometry. While the high optical-polishing quality can lead to the similar high Q, such box resonator differs from the WGMR as a waveguide-based resonator to be easily end-coupled, and most importantly coat-configurable for noncritical frequency matching in OPO. The simulated TM00 mode profile of box resonator is shown at the top right of Fig. 1(c). The four polished sidewalls ensure low loss total internal reflection for optical waves propagation while the two end faces are coating configurable. The fabrication process is shown in Fig. 1(b). It starts from a z-cut MgO-doped lithium niobate (LN) optical superlattice crystal [35–37] with poling period of 30.4 μm for type-0 quasiphase matched OPO from 1054 to 1546 nm and 3310 nm at 356 K. This crystal is grinded into thin film and finely polished down to a thickness of 110 μm. Lithium tantalate (LT) substrates are bonded on both sides of the optical superlattice thin film for surface protection and thermal management, with 100 nm thick SiO_2 layer deposited on each bonding surface as buffer material. The cross-section facets are then polished and dielectrically coated with 99.8% (for $S1$) and 99% (for $S2$) reflection, respectively, at around 1.5 μm and antireflection at 1.0 μm and 3 μm. Multiple box resonator devices can be achieved by the slicing and sidewall polishing from sandwiched thin film, with a width of 0.49 mm. Finally, a 0.3 mm thick LT sheet is bonded to the rear facet ($S2$) of box resonator, with a third reflective facet ($S3$) coated with 90% reflection around 1.5 μm, for single longitudinal mode selection.

We characterize the Q of box resonator by scanning the frequency of a 1.5 μm tunable semiconductor laser

(TSL, Toptica CTL1550) over the resonances of TM mode, i.e., the extraordinary polarization. As shown in Fig. 1(c), the free spectral range (FSR) is 1.47 GHz, in good agreement with the 45.5 mm length of the box resonator. The linewidth of TM00 mode is fitted to be 8.4 MHz, which corresponds to $2.3 \times 10^7 Q$. Such high Q is comparable to that of WGMRs [38,39], as expected, and is the key to enabling low threshold even in a mini-OPO scheme with such large mode area, as required for high-power handling. It is worth noting that although the relatively large mode area results in multitransverse modes, only low-order modes are in high Q due to their less sensitivity to the surface roughness, and mode-selective excitation is possible with the adjustment of free space-to-resonator coupling. And the large mode area and straight-waveguide design of box resonator also lead to neglectable dispersion deviation from bulk LN crystal with effective refraction indices variations less than 10^{-5} at all wavelengths, so that we can take advantage of the mature quasiphase matching and periodical poling technologies in bulk crystal.

The schematic of the experimental setup is shown in Fig. 2(a). We use an ytterbium-doped fiber amplifier (YDFA) amplified 1 μm TSL (Toptica CTL1050) as pump. The pump beam is directed through a set of cylindrical lenses to match the profile of the TM00 mode. Filters are used to separate the pump, signal, and MIR idler beams for further measurement. The box resonator is placed on a doubly enclosed temperature-controlled metal mount with instability of about 2 mK. For our box resonator based OPO, the pump intensity required to reach oscillation threshold can be expressed as [40]

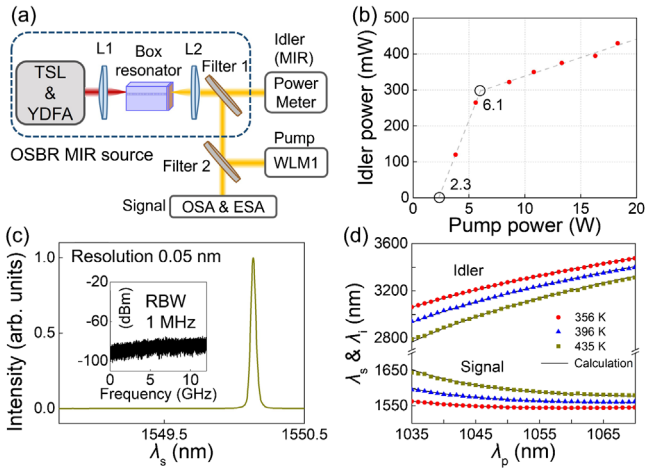

FIG. 2. Power and wavelength tuning of the box resonator. (a) Experimental setup. WLM, wavelength meter; $L1$, $L2$, sets of cylindrical lenses. (b) The MIR output power as a function of pump power. (c) The linear-scale spectrum of signal wave shows a clean single peak. The inset shows the result of a rf measurement, to confirm a single-longitudinal-mode oscillation. RBW, resolution bandwidth. (d) Wavelengths of signal and idler light as a function of the pump wavelength.

$$I_{\mathrm{th}} = \frac{c\varepsilon_0 n_p n_s n_i \lambda_s \lambda_i \alpha_s}{8\pi^2 L^2 d_{\mathrm{eff}}^2}, \tag{2}$$

where ε_0 and λ are the dielectric constant and wavelength in vacuum, respectively, n and $d_{\mathrm{eff}} = 14.8$ pm/V are the refractive index and effective nonlinear coefficient of LN, respectively, the subscripts p, s, i represent for pump, signal, and idler waves, α_s is the fractional round-trip power loss for the signal wave. Figure 2(b) shows the MIR output power as a function of pump power with the conversion efficiency up to 4.7%. The oscillation threshold can be estimated to be about 2.3 W, which matches well with the theoretical value of 1.9 W considering the additional coupling loss of pump beam. The kink in this curve at 2.7 times threshold is due to the saturation of the pump depletion. The maximum MIR output power is 0.43 W with pump power of 18.3 W, which is important for high-sensitivity long-distance methane sensing and beyond the current capability of the quantum cascade lasers at this wavelength.

The spectrum of the signal light is measured by an optical spectrum analyzer (OSA, Yokogawa Electric Corp. AQ6375) as plotted in Fig. 2(c), showing a clean single peak, within the instrument limited resolution (0.05 nm, corresponding to 6.2 GHz at 1550 nm) of OSA. The radio frequency (rf) measurement result in electrical spectrum analyzer (ESA) produced by sending the signal beam to a fast photodetector (PD, EOT, ET-5000F) shows no identifiable rf noise in the range from DC to 12 GHz [inset of Fig. 2(c)]. These results confirm single-longitudinal-mode optical parametric oscillation for the signal light, and thus the MIR idler light as well.

Figure 2(d) shows the wavelength tuning results with pump wavelength tuning at different temperatures of box resonator. For OPO process, the functional relationship of signal, idler, and pump wavelengths under different temperature (T) can be extracted from energy conservation and momentum conservation as

$$\frac{n(\lambda_p, T)}{\lambda_p} = \frac{n(\lambda_s, T)}{\lambda_s} + \frac{n(\lambda_i, T)}{\lambda_i} + \frac{1}{\Lambda}, \tag{3}$$

where Λ is the poling period of LN and $n(\lambda, T)$ is temperature-dependent Sellmeier equation for LN crystal [41]. The measurement results match well with the calculated tuning curves. Single-frequency MIR output can be achieved in a wide wavelength range from 2800 to 3400 nm.

In MIR spectroscopy applications, the laser linewidth defines the spectral resolution, and narrow linewidth and high spectral accuracy are the keys for the characterization for the fine and hyperfine absorption features of molecules. In fact, the direct linewidth measurement for such a high-quality MIR source can be a challenge that requires MIR interferometry, so that we perform an indirect measurement for the signal light, and MIR linewidth can be inferred from energy conservation. Such measurement is performed using

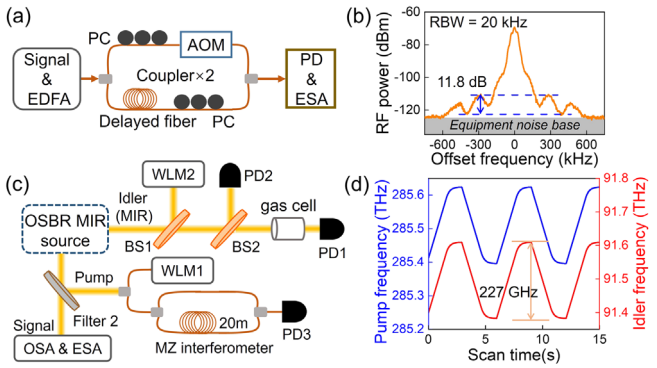

FIG. 3. Characterizations of linewidth and continuous tuning ability. (a) Schematic of experimental setup for linewidth measurement. (b) Measured coherent envelope, showing a CDSPST of 11.8 dB. (c) Experiment setup for mod-hop-free tuning measurement and low-pressure methane absorption spectrum measurement. BS, beam splitter. (d) Both pump (blue curve) and idler (red curve) frequencies are recorded by two wavelength meters, respectively, showing a mode-hop-free tuning range up to 227 GHz.

short delayed self-heterodyne interferometry (SDSHI), where the signal light linewidth can be estimated from the strong coherent envelope in the self-heterodyne rf beat signal [42,43]. As shown in Fig. 3(a), the signal light is first amplified in an erbium-doped fiber amplifier (EDFA) and then directed to two interferometer arms by a 1×2 fiber coupler. The light in the upper arm is frequency shifted by 40 MHz using an acoustic optical modulator (AOM), while that in lower arm is directed through 1 km of fiber delay. The lights in the two interferometer arms are then recombined using a second 1×2 fiber coupler, and detected by a PD at the output port. Polarization controllers (PCs) are aligned to maximize the fringe contrast of the interference and thus the signal-to-noise ratio of the rf beat note. Figure 3(b) shows the measurement result, and signal linewidth can be retrieved from the contrast difference between the second peak and the second trough (CDSPST, ΔS) in the coherent envelope, using the following equation [42,43]:

$$\Delta S(\Delta f) = 10\log_{10}\frac{\left[1+\left(\frac{2c}{n_f \Delta f L_f}\right)^2\right]\left[1+e^{-2\pi\frac{n_f \Delta f L_f}{c}}\right]}{\left[1+\left(\frac{3c}{2n_f \Delta f L_f}\right)^2\right]\left[1-e^{-2\pi\frac{n_f \Delta f L_f}{c}}\right]}, \quad (4)$$

where n_f and L_f are the refractive index and length of delayed fiber, respectively, and Δf is the Lorentzian linewidth of the power spectrum. Here, the measured CDSPST is estimated to be 11.8 dB, corresponding to a signal linewidth of 7.7 kHz according to Eq. (4), which is on the same order as the pump linewidth of ~5 kHz (according to manufacturer's data). Therefore, the MIR linewidth of 10 kHz maximum can be estimated.

The commercial visible/NIR tunable lasers are known for their large mode-hop-free tuning ranges. Our box resonator is designed to transfer such feature to the MIR range in a mini-OPO platform. A high-fidelity transfer can be achieved in our box resonator geometry while the signal wavelength is self-locked to the center of the same longitudinal mode during the whole pump tuning. We track such frequency transfer from the NIR to MIR wavelength, by the direct wavelength samplings on the NIR pump and MIR idler simultaneously, using two wavelength meters (WLM, HighFinesse, pump: WSU-2, and MIR: WS6-200 IR-III), as shown in Fig. 3(c). Consistent and uniform MIR tuning is achieved following the pump tuning within a wide mode-hop-free tuning range of 227 GHz [29] as shown in Fig. 3(d). Considering the limited sampling rates of the WLMs, a relatively low pump tuning speed of 73 GHz/s is used. Such wide tuning range benefits from the noncritical frequency matching in box resonator geometry as well as the single longitudinal mode enhancement by the LT etalon.

To further test the frequency consistency in fine absorption features characterization using our box resonator-based MIR source, we perform a spectrum measurement on the low-pressure methane, where each absorption line can be well referenced to the theoretical calculation [44]. The MIR wavelength is set around 3315 nm (or 3017 cm^{-1} in wave number), for the investigation of Q branch in the methane v_3 band [45,46]. These major lines are known as the methane fingerprints, but at the short wavelength edge for the quantum cascade laser (QCL) technology from the fabrication point of view [47–49]. Here, we use a 30-cm long gas cell containing 0.15 mbar of methane buffered to 0.57 mbar nitrogen to minimum the collision broadening of the absorption lines. Most of the MIR output is directed through the gas cell to a PD for the transmission measurement, while a small portion of the MIR output is directly sent to a second PD for the intensity normalization. We also correct the pump tuning uniformity by a clock signal, that is generated from a fiber Mach-Zehnder interferometer (MZI) using a small portion of pump light, as shown in Fig. 3(c). The MZI is built with 20 m unbalanced path lengths, which results in a 10.3 MHz interference clock rate.

With pump tuning rate at 1 THz/s, we perform the measurement over the frequency span of 110 GHz (3.7 cm^{-1}) and the results (blue curves) are shown in Fig. 4(a) in comparison to the theoretical calculation [44]. The well-matched absorption lines are clearly visualized as the close-up view shown in Fig. 4(b), with calculated small inaccuracy of 1.84 MHz maximum and 0.97 MHz root-mean-square (rms) [navy dots in Fig. 4(c)], which can be further improved by stabilizing the fiber delay line in the MZI [50]. We further perform the residual of the measured data from the theoretical calculation [magenta curve in Fig. 4(c)], and low rms value of 0.0089 is calculated. Notably, these results indicate that this mini-OPO MIR source can distinguish individual features in complex and possibly overlapping spectra for real-time spectroscopic

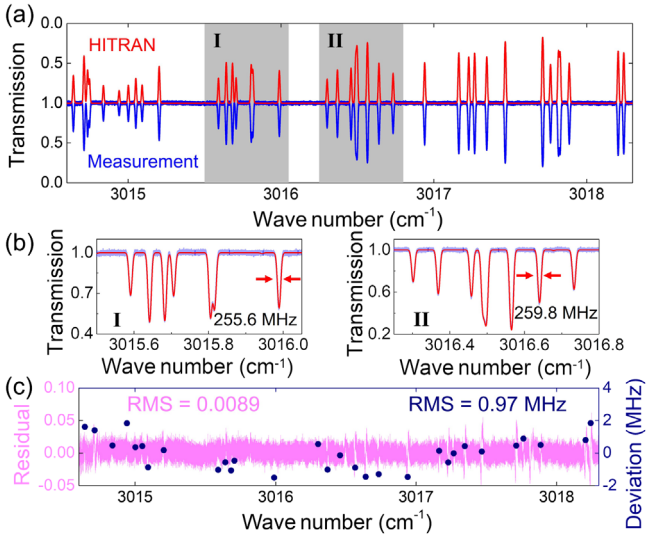

FIG. 4. Low-pressure methane absorption spectrum measurement. (a) Experimentally measured and theoretically calculated MIR transmissions from gas cell are plotted in blue and red curves, respectively. (b) Detailed gas absorbance trace of the highlighted regions in (a). (c) The residual values (magenta curve) and the peaks in accuracy (navy dots) from the theoretical calculation.

analysis, since the spectral resolution is better than the width of molecular absorption considering the typical pressure-broadening of the spectral lines.

In conclusion, we have demonstrated a box resonator mini-OPO and resolve the critical frequency matching problem in normal monolithic OPO schemes. Such box resonator geometry is the second type of mini-OPO to achieve material-limited high Q in parallel to the WGMR for lithium niobate, but with noncritical frequency matching for stable free-running operation and continuous tuning. High-fidelity NIR to MIR frequency conversation is achieved, not only at single frequency, but also in mode-hop-free tuning, and without critical temperature stabilization and pump-to-resonance matching requirement. MHz-level high accuracy and 10-kHz high resolution are achieved in the continuous tuning range up to 227 GHz. With MIR output designed around 3.3 μm, the high spectroscopy performance is harnessed with the fine structure measurement using low-pressure methane, and can be generalized to other MIR wavelengths with different domain engineering of the optical superlattice. In this work, we use a high-performance external cavity diode laser as a pump to study the performance limit of our box resonator-based MIR source. In practical applications, chip-scale pump sources, for example a DFB laser diode, can be used for more compact size, better environment robustness, and lower cost of the system, for field-deployable devices. Here, we use a box resonator with 110 μm thickness to enable 430 mW high-power MIR output, direct diode pump without fiber amplifier is possible with thinner box resonator design down to the 10-μm level, in an even smaller package for low power applications.

We thank Professor Rong Zhang for assistance with the gas preparation, and Professor Xiaoshun Jiang for stimulating discussions. We acknowledge the support by the National Key R&D Program of China (2019YFA0705000, 2017YFA0303700), National Natural Science Foundation of China (51890861, 11690031, 11621091, 11674169), Leading-edge technology Program of Jiangsu Natural Science Foundation (BK20192001), Key R&D Program of Guangdong Province (2018B030329001), Guangdong Major Project of Basic and Applied Basic Research, and Jiangsu Planned Projects for Postdoctoral Research Funds.

*These authors contributed equally to this work.
†xiezhenda@nju.edu.cn
‡zhusn@nju.edu.cn

[1] E. D. Hinkley, A. R. Calawa, P. L. Kelley, and S. A. Clough, Tunable-laser spectroscopy of the ν_1 band of SO_2, J. Appl. Phys. **43**, 3222 (1972).
[2] F. J. Duarte, *Tunable Laser Applications* (CRC Press, New York, 2008).
[3] R. K. Hanson, P. A. Kuntz, and C. H. Kruger, High-resolution spectroscopy of combustion gases using a tunable IR diode laser, Appl. Opt. **16**, 2045 (1977).
[4] W. Demtröder, *Laser Spectroscopy: Basic Concepts and Instrumentation* (Springer, New York, 2013).
[5] J. Cousin, P. Masselin, W. Chen, D. Boucher, S. Kassi, D. Romanini, and P. Szriftgiser, Application of a continuous-wave tunable erbium-doped fiber laser to molecular spectroscopy in the near infrared, Appl. Phys. B **83**, 261 (2006).
[6] J. Hult, I. S. Burns, and C. F. Kaminski, Wide-bandwidth mode-hop-free tuning of extended-cavity GaN diode lasers, Appl. Opt. **44**, 3675 (2005).
[7] D. K. Shin, B. M. Henson, R. I. Khakimov, J. A. Ross, C. J. Dedman, S. S. Hodgman, K. G. H. Baldwin, and A. G. Truscott, Widely tunable, narrow linewidth external-cavity gain chip laser for spectroscopy between 1.0–1.1 μm, Opt. Express **24**, 27403 (2016).
[8] H. Shawki, H. Kotb, and D. Khalil, Single-longitudinal-mode broadband tunable random laser, Opt. Lett. **42**, 3247 (2017).
[9] B. Stern, X. Ji, A. Dutt, and M. Lipson, Compact narrow-linewidth integrated laser based on a low-loss silicon nitride ring resonator, Opt. Lett. **42**, 4541 (2017).
[10] I. T. Sorokina and K. L. Vodopyanov, *Solid-State Midinfrared Laser Sources* (Springer, New York, 2003).
[11] A. Godard, Infrared (2–12 μm) solid-state laser sources: A review, C R Phys **8**, 1100 (2007).
[12] M. Ebrahim-Zadeh and I. T. Sorokina, *Midinfrared Coherent Sources and Applications*, (Springer, New York, 2007).
[13] H. Ishizuki and T. Taira, High-gain midinfrared optical-parametric generation pumped by microchip laser, Opt. Express **24**, 1046 (2016).
[14] M. W. Haakestad, G. Arisholm, E. Lippert, S. Nicolas, G. Rustad, and Knut Stenersen, High-pulse-energy midinfrared

laser source based on optical parametric amplification in $ZnGeP_2$, Opt. Express **16**, 14263 (2008).
[15] W. R. Bosenberg, A. Drobshoff, J. I. Alexander, L. E. Myers, and R. L. Byer, 93% pump depletion, 3.5-W continuous-wave, singly resonant optical parametric oscillator, Opt. Lett. **21**, 1336 (1996).
[16] L. E. Myers, G. D. Miller, R. C. Eckardt, M. M. Fejer, R. L. Byer, and W. R. Bosenberg, Quasi-phase-matched 1.064-μm-pumped optical parametric oscillator in bulk periodically poled $LiNbO_3$, Opt. Lett. **20**, 52 (1995).
[17] W. R. Bosenberg, A. Drobshoff, J. I. Alexander, L. E. Myers, and R. L. Byer, Continuous-wave singly resonant optical parametric oscillator based on periodically poled $LiNbO_3$, Opt. Lett. **21**, 713 (1996).
[18] E. Lippert, H. Fonnum, G. Arisholm, and K. Stenersen, A 22-watt midinfrared optical parametric oscillator with V-shaped 3-mirror ring resonator, Opt. Express **18**, 26475 (2010).
[19] H. Y. Clark, L. Corner, W. Denzer, G. Hancock, A. Hutchinson, M. Islam, R. Peverall, and G. A. D. Ritchie, Difference frequency generation in periodically poled lithium niobate and its use in the detection of atmospheric methane, Chem. Phys. Lett. **399**, 102 (2004).
[20] T. Beckmann, H. Linnenbank, H. Steigerwald, B. Sturman, D. Haertle, K. Buse, and I. Breunig, Highly Tunable Low-Threshold Optical Parametric Oscillation in Radially Poled Whispering Gallery Resonators, Phys. Rev. Lett. **106**, 143903 (2011).
[21] J. U. Fürst, D. V. Strekalov, D. Elser, A. Aiello, U. L. Andersen, C. Marquardt, and G. Leuchs, Low-Threshold Optical Parametric Oscillations in a Whispering Gallery Mode Resonator, Phys. Rev. Lett. **105**, 263904 (2010).
[22] Z. D. Xie, X. J. Lv, Y. H. Liu, W. Ling, Z. L. Wang, Y. X. Fan, and S. N. Zhu, Cavity Phase Matching via an Optical Parametric Oscillator Consisting of a Dielectric Nonlinear Crystal Sheet, Phys. Rev. Lett. **106**, 083901 (2011).
[23] Q. Mo, S. Li, Y. Liu, X. Jiang, G. Zhao, Z. Xie, X. Lv, and S. Zhu, Widely tunable optical parametric oscillator in periodically poled congruently grown lithium tantalite whispering gallery mode resonators, Chin. Optic. Lett. **14**, 091902 (2016).
[24] B. Way, R. K. Jain, and M. Hossein-Zadeh, High-Q microresonators for mid-IR light sources and molecular sensors, Opt. Lett. **37**, 4389 (2012).
[25] P. Ma, D.-Y. Choi, Y. Yu, Z. Yang, K. Vu, T. Nguyen, A. Mitchell, B. Luther-Davies, and S. Madden. High Q factor chalcogenide ring resonators for cavity-enhanced MIR spectroscopic sensing, Opt. Express **23**, 19969 (2015).
[26] C. Lecaplain, C. Javerzac-Galy, M. L. Gorodetsky, and T. J. Kippenberg, Midinfrared ultra-high-Q resonators based on fluoride crystalline materials, Nat. Commun. **7**, 13383 (2016).
[27] T.-H. Xiao, Z. Zhao, W. Zhou, C.-Y. Chang, S. Y. Set, M. Takenaka, H. K. Tsang, Z. Cheng, and K. Goda, Midinfrared high-Q germanium microring resonator, Opt. Lett. **43**, 2885 (2018).
[28] S. A. Miller, M. Yu, X. Ji, A. G. Griffith, J. Cardenas, A. L. Gaeta, and M. Lipson, Low-loss silicon platform for broadband midinfrared photonics, Optica **4**, 707 (2017).
[29] I. D. Lindsay, B. Adhimoolam, P. Gross, M. E. Klein, and K. J. Boller, 110 GHz rapid, continuous tuning from an optical parametric oscillator pumped by a fiber-amplified DBR diode laser, Opt. Express **13**, 1234 (2005).
[30] M. E. Klein, P. Gross, K. J. Boller, M. Auerbach, P. Wessels, and C. Fallnich, Rapidly tunable continuous-wave optical parametric oscillator pumped by a fiber laser, Opt. Lett. **28**, 920 (2003).
[31] M. E. Klein, C. K. Laue, D. H. Lee, K. J. Boller, and R. Wallenstein, Diode-pumped singly resonant continuous-wave optical parametric oscillator with wide continuous tuning of the near-infrared idler wave, Opt. Lett. **25**, 490 (2000).
[32] M. Siltanen, M. Vainio, and L. Halonen, Pump-tunable continuous-wave singly resonant optical parametric oscillator from 2.5 to 4.4 μm, Opt. Express **18**, 14087 (2010).
[33] I. D. Lindsay, P. Groß, C. J. Lee, B. Adhimoolam, and K.-J. Boller, Midinfrared wavelength- and frequency-modulation spectroscopy with a pump-modulated singly-resonant optical parametric oscillator, Opt. Express **14**, 12341 (2006).
[34] M. Vainio, M. Siltanen, J. Peltola, and L. Halonen, Grating-cavity continuous-wave optical parametric oscillators for high-resolution midinfrared spectroscopy, Appl. Opt. **50**, A1 (2011).
[35] S. N. Zhu, Y. Y. Zhu, and N. B. Ming, Quasi-phase-matched third-harmonic generation in a quasi-periodic optical superlattice, Science **278**, 843 (1997).
[36] H. Jin *et al.*, On-Chip Generation and Manipulation of Entangled Photons Based on Reconfigurable Lithium-Niobate Waveguide Circuits, Phys. Rev. Lett. **113**, 103601 (2014).
[37] Y. W. Lee, F. C. Fan, Y. C. Huang, B. Y. Gu, B. Z. Dong, and M. H. Chou, Nonlinear multiwavelength conversion based on an aperiodic optical superlattice in lithium niobate, Opt. Lett. **27**, 2191 (2002).
[38] K. J. Vahala, Optical microcavities, Nature (London) **424**, 839 (2003).
[39] A. A. Savchenkov, V. S. Ilchenko, A. B. Matsko, and L. Maleki, Kilohertz optical resonances in dielectric crystal cavities, Phys. Rev. A **70**, 051804(R) (2004).
[40] M. Ebrahimzadeh and M. H. Dunn, *Optical parametric oscillators, in Handbook of Optics* (McGraw-Hill, New York, 2001).
[41] O. Gayer, Z. Sacks, E. Galun, and A. Arie, Temperature and wavelength dependent refractive index equations for MgO-doped congruent and stoichiometric $LiNbO_3$, Appl. Phys. B **91**, 343 (2008).
[42] S. Huang, T. Zhu, M. Liu, and W. Huang, Precise measurement of ultra-narrow laser linewidths using the strong coherent envelope, Sci. Rep. **7**, 41988 (2017).
[43] S. Huang, T. Zhu, Z. Cao, M. Liu, M. Deng, J. Liu, and X. Li, Laser linewidth measurement based on amplitude difference comparison of coherent envelope, IEEE Photonics Technol. Lett. **28**, 759 (2016).
[44] I. E. Gordon *et al.*, The HITRAN2016 molecular spectroscopic database, J Quant Spectrosc Radiat. Transf. **203**, 3 (2017).
[45] D. R. J. Boyd, H. W. Thompson, and R. L. Williams, Vibration-rotation bands of methane, Proc. Math. Phys. Eng. Sci. **213**, 42 (1952).

[46] D. L. Gray, A. G. Robiette, and A. S. Pine, Extended measurement and analysis of the $\nu 3$ infrared band of methane, J. Mol. Spectrosc. **77**, 440 (1979).

[47] A. Hugi, G. Villares, S. Blaser, H. C. Liu, and J. Faist, Midinfrared frequency comb based on a quantum cascade laser, Nature (London) **492**, 229 (2012).

[48] Y. Yao, A. Hoffman, and C. Gmachl, Midinfrared quantum cascade lasers, Nat. Photonics **6**, 432 (2012).

[49] N. Bandyopadhyay, Y. Bai, S. Tsao, S. Nida, S. Slivken, and M. Razeghi, Room temperature continuous wave operation of $\lambda \sim 3$–3.2 μm quantum cascade lasers, Appl. Phys. Lett. **101**, 241110 (2012).

[50] D. Kwon, I. Jeon, W. K. Lee, M. S. Heo, and J. Kim, Generation of multiple ultrastable optical frequency combs from an all-fiber photonic platform, Sci. Adv. **6**, eaax4457 (2020).